

## Comparison study of the effect of blending method on PVDF/PPTA blend membrane structure and performance

Hongbin Li<sup>\*1</sup>, Wenyong Shi<sup>1</sup>, Yufeng Zhang<sup>2</sup> and Rong Zhou<sup>1</sup>

<sup>1</sup> School of Textiles Engineering, Henan Institute of Engineering, Zhengzhou, 450007, P.R. China

<sup>2</sup> State Key Laboratory of Hollow Fiber Membrane Materials and Processes, School of Materials Science and Engineering, Tianjin Polytechnic University, Tianjin 300387, P.R. China

(Received March 28, 2014, Revised January 17, 2015, Accepted January 21, 2015)

**Abstract.** A novel hydrophilic poly (vinylidene fluoride)/poly (*p*-phenylene terephthalamide) (PVDF/PPTA) blend membrane was prepared by *in situ* polycondensation of *p*-phenylene diamine (PPD) and terephthaloyl chloride (TPC) in PVDF solution with subsequent nonsolvent induced phase separation (NIPS) process. For comparison, conventional solution blend membrane was prepared directly by adding PVDF powder into PPTA polycondensation solution. Blend membranes were characterized by means of viscometry, X-ray photoelectron spectroscopy (XPS), Field Emission Scanning Electron Microscopy (FESEM). The effects of different blending methods on membrane performance including water contact angle (WCA), mechanical strength, anti-fouling and anti-compression properties were investigated and compared. Stronger interactions between PVDF and PPTA in *in situ* blend membranes were verified by viscosity and XPS analysis. The incorporation of PPTA accelerated the demixing rate and caused the formation of a more porous structure in blend membranes. *In situ* blend membranes exhibited better hydrophilicity and higher tensile strength. The optimal values of WCA and tensile strength were 65° and 34.1 MPa, which were reduced by 26.1% and increased by 26.3% compared with pure PVDF membrane. Additionally, antifouling properties of *in situ* blend membranes were greatly improved than pure PVDF membrane with an increasing of flux recovery ratio by 25%. Excellent anti-compression properties were obtained in *in situ* blend membranes with a stable pore morphology. The correlations among membrane formation mechanism, structure and performance were also discussed.

**Keywords:** *in situ* polycondensation; PVDF membrane; PPTA; hydrophilicity; mechanical strength; anti-fouling; anti-compression

### 1. Introduction

Poly (vinylidene fluoride) (PVDF) has been widely used as a microfiltration and ultrafiltration membrane material due to its excellent film-forming property, thermal stability and chemical resistance (Madaeni *et al.* 2011). However, its high hydrophobicity and poor antifouling properties restrict its application in wastewater treatments especially in membrane bioreactor (MBR) (Pang *et al.* 2011). Besides, dimension shrinkage, even membrane rupture would happen during long-term aeration operation with activated sludge (Yuliwati *et al.* 2011). Currently, hydrophilic modification

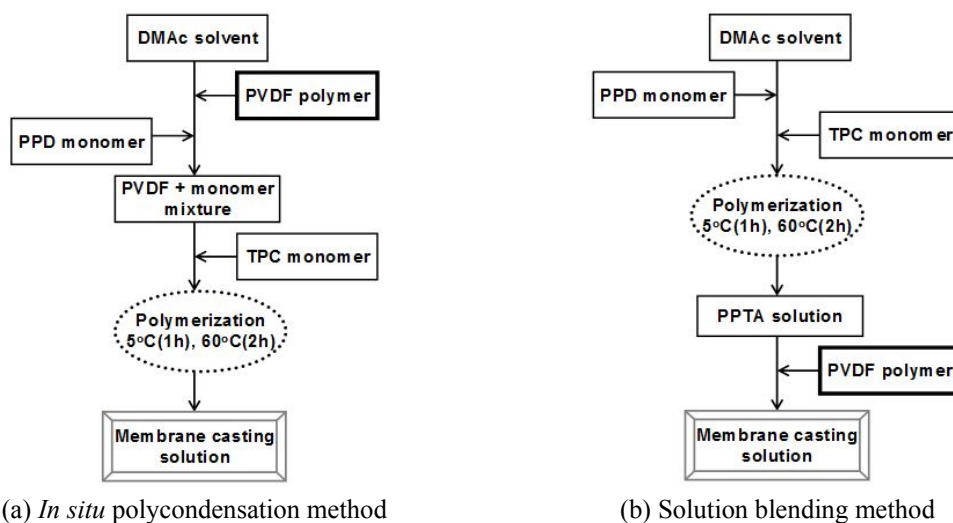
---

\*Corresponding author, Ph.D., E-mail: [lihongbin20033421@163.com](mailto:lihongbin20033421@163.com)

of PVDF membranes has been one of the hotspots in membrane science (Liu *et al.* 2011). Surface modification (including surface coating and grafting) and blending modification have been explored to overcome these limitations (Hegde *et al.* 2012). Nevertheless, a loss of active groups would occur via surface coating method due to the weak adhesion between coating layer and membrane substrate along a long-term filtration and cleaning process. In addition, mechanical strength of membrane substrate cannot be enhanced simultaneously by these two methods (Nasef and Hegazy 2004, Hashim *et al.* 2012). More importantly, most of surface modification techniques are focused on flat sheet membranes, which limited their developments in hollow fiber membrane modifications. For conventional blending method, microscopic phase separation often emerges in blend membranes due to thermodynamic difference between the modifier and polymer matrix, which results in poor macroscopic performance of membranes (Zhao *et al.* 2007).

A novel blending method named *in situ* polymerization combined modification with membrane preparation process is developed as a desirable method to prepare hydrophilic PVDF blend membranes. Hydrophilic oligomers or monomers are mixed sufficiently with PVDF molecules prior to the polymerization reaction. Hydrophilic modifier could be dispersed well at molecular level in the PVDF matrix. Thus, compatible blend membranes could be obtained by this method (Ji *et al.* 2005, Woo *et al.* 2003). Blend membranes prepared by *in situ* polymerization technique have been successfully applied in the fabrication of proton exchange membranes (PEM) (Feng *et al.* 2010, Huang *et al.* 2012, Fu *et al.* 2007, Han *et al.* 2011), and gas separation membranes (Vaughan *et al.* 2008). These studies have fully confirmed that excellent membrane performance can be obtained via *in situ* polymerization. Recent researches have focused on *in situ* free radical polymerization to improve the hydrophilic and antifouling properties of PVDF membrane. Oligomers such as 2-hydroxyethyl methacrylate (HEMA) (Liu *et al.* 2012a), polyethylene glycol monomethyl ether methyl methacrylate (PEGMA) and methyl methacrylate (MMA) (Zhang *et al.* 2013) are polymerized by the initiator azodiisobutyronitrile (AIBN) in PVDF solution. However, there are few reports on using *in situ* polycondensation technique to prepare PVDF modified membranes and less emphasis was placed on the compatibility between hydrophilic polymer and PVDF matrix as well as its effects on membrane performance. In this work, poly (*p*-phenylene terephthalamide) (PPTA) was selected as the hydrophilic modifier due to its excellent mechanical strength, hydrophilicity and dimensional stability to improve the hydrophilicity and mechanical properties of PVDF membranes (Rao *et al.* 2001, Knijnenberg *et al.* 2010). So far, few studies have been investigated on the preparation of PPTA blend membrane. The main reason is the refractory and insolubility of PPTA in common solvents. Blending through *in situ* polycondensation can solve these problems. Monomers of PPTA can be dissolved well in PVDF solution followed by polycondensation under suitable conditions and the synthetic solution can be directly used as membrane casting solution.

In this study, *in situ* polycondensation and conventional solution blending were compared for the synthesis of PVDF/PPTA casting solution and inversion phase separation method was used to prepare hydrophilic PVDF/PPTA blend membranes. The procedure of *in situ* polycondensation was illustrated in Scheme 1(a). PPD and TPC monomers reacted in PVDF solution at low temperature. Solution blending was implemented by adding PVDF powders into PPTA polycondensation solution as shown in Scheme 1(b). The effect of these two methods on polymer compatibility and membrane performance were systematically investigated, compared and analyzed. Polymer compatibilities in different blend membranes were compared through viscometry, XPS and FESEM observation. Membrane performance was evaluated by hydrophilicity, mechanical strength, anti-fouling and anti-compression properties measurements.



Scheme 1 Flow chart of the preparation of blend membrane casting solution

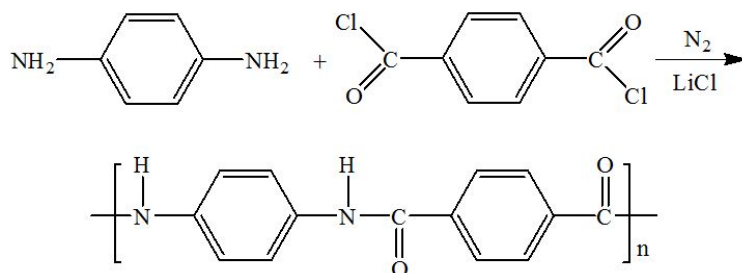
## 2. Experimental

### 2.1 Materials

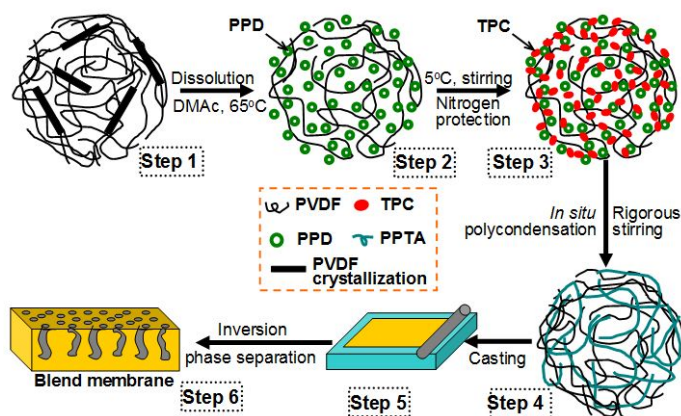
PVDF (FR-904,  $\eta_{inh} = 1.6$  dL/g) powder was supplied by Shanghai 3F New Materials Co., Ltd. (Shanghai, China), and dehydrated in a vacuum oven at 80°C for 12 h. PPD (purity  $\geq 99\%$ ), TPC (purity  $\geq 99\%$ ), anhydrous LiCl (purity  $\geq 99\%$ ), bovine serum albumin (BSA) and *N,N*-dimethyl acetamide (DMAc, purity  $\geq 99\%$ ) were all purchased from Aladdin Chemical Co., Ltd. (Shanghai, China). Other reagents were all AR grade and used without any treatment. PPTA was synthesized by low temperature solution polycondensation of PPD and TPC in DMAc solution. The specific synthetic route of PPTA was shown in Scheme 2.

### 2.2 Synthesis of membrane casting solution

All glass vessels were cleaned and heated to remove any organic or moisture residue prior to be used. *In situ* polycondensation conditions for the synthesis of casting solution are proposed in



Scheme 2 The synthetic route of PPTA



Scheme 3 Scheme of blend membrane preparation procedures via in situ polycondensation

Scheme 3. Semi-crystalline PVDF (step 1) and latent solvent LiCl (2wt%) powders were dissolved in DMAC (84 wt%) at 65°C. PPD monomer was dispersed in PVDF solution to form a homogenous solution (step 2) at atmosphere temperature. Then, TPC monomer (TPC/PPD = 1.007/1, molar ratio) was rapidly added into PVDF/PPD monomer mixture (step 3) at 5°C under rigorous stirring (3000 r/min). After reacting for 60 min, system temperature was increased to 60°C for further polycondensation for 2 h and membrane casting solution could be obtained (step 4). The difference between solution blending and *in situ* polycondensation was the feeding sequence of PVDF. For solution blending, PVDF powder was introduced into reaction system after the completion of PPTA polycondensation. Polymer concentration was fixed at 14wt%. The blending ratio of PVDF/PPTA varied in the range of 90/10, 80/20, 70/30 and 60/40 with an appropriate casting solution viscosity. Both casting solution synthesized by *in situ* polycondensation and corresponding membranes were named as PA-10, PA-20, PA-30 and PA-40. The casting solution obtained through solution blending and corresponding membranes with the same PPTA concentration were noted as SPA-10, SPA-20, SPA-30 and SPA-40. Besides, pure PVDF membrane and PPTA particles were named as PA-0 and PA-100, respectively. The PPTA content mentioned in this paper referred to the PPTA mass fraction in PVDF/PPTA blends. The viscosities of different casting solution were measured by a viscometer (RVDV-II+P, Brookfield engineering laboratories, USA) at 25°C.

### 2.3 Membrane preparation

Blend membranes were prepared via NIPS technique. Casting solution was cast onto glass plates at ambient temperature using a stainless steel casting knife with a gap distance of 250  $\mu\text{m}$  (Scheme 3 step 5). Then, the plates were immersed into water coagulation bath to prepare porous blend membranes (Scheme 3 Step 6). Nascent membranes were cleaned with deionized water several times and then stored in 5wt%  $\text{NaHSO}_3$  aqueous solution.

### 2.4 Membrane surface characterization

Fourier transform infrared spectra (FTIR) of different blends were recorded through a FTIR TENSOR 37 (BRUKER Corporation, Germany) operated by Attenuated Total Reflectance (ATR)

in wave number range of 3000-400  $\text{cm}^{-1}$ . The content of O, F, N, C elements on membrane surface was examined by X-ray photoelectron spectroscopy (XPS) measurement (Quanta 200 spectrometer, FEI Co., Ltd. USA). Survey spectra were run in the binding energy range 0-1350 eV. Surface and cross-section morphologies of membranes were observed by field emission scanning electron microscopy (FESEM, Hitachi S-4800, Japan) under high vacuum condition. Membrane samples were cut into appropriate size and sputter-coated with gold prior to the FESEM measurements. The water contact angle (WCA) value of membrane surface was implemented on a Kruss Instrument (CM3250-DS3210, Germany) at ambient temperature to evaluate wetting ability of different blend membranes. To ensure that the results were sufficiently credible, the WCA values were the average of five measurements on different locations.

### 2.5 Membrane hydration capability and shrinkage ratio

Hydration capabilities ( $\text{mg}/\text{cm}^3$ ) of membranes were determined through the weight measurement of wet membranes and dry membranes. Dry membrane samples with a diameter of 3cm were first weighed using a precision balance. Then, the samples were immersed in deionized water for 24h. Afterwards, membranes were wiped out with filter paper, and the weight was also obtained. Hydration capability was evaluated taking the weight difference of dry and wet membranes per unit volume. For each membrane, five independent measurements were carried out and the average value of membrane hydration capability was obtained.

Before casting, glass plate was firstly mark with fixed length and width. After the casting, the casting solution outside the marked area on glass plate was immediately scrapped off through the steel ruler. Then, the glass plate was immersed instantly into the water coagulation bath. Membrane shrinkage ratio was defined as

$$S = \left( 1 - \frac{M_1}{M_0} \right) \times 100\% \quad (1)$$

Where  $M_0$  and  $M_1$  were the membrane area before and after membrane solidification, respectively.

### 2.6 Porosity and average pore size

Membrane porosity ( $\varepsilon$ ) was estimated from the mass loss of wet membrane after drying. Membrane samples were weighed under wet and dry conditions. The ratio of pore volume to membrane geometrical volume was defined as Eq. (2)

$$\varepsilon = \frac{(W_w - W_d)}{Al\rho} \quad (2)$$

Where  $W_w$  and  $W_d$  were the weights of membranes (g) at the wet swelling and dry state, respectively.  $A$ ,  $L$ , and  $\rho$  were the sample area ( $\text{cm}^2$ ), average thickness (cm) and pure water density at atmosphere temperature ( $\text{g}/\text{cm}^3$ ).

The average effective through-pore size and pore volumes of blend membranes were measured by means of a capillary Flow Porometer CFP 1500 AEXL (Porous materials Inc., USA) as described before (Shi *et al.* 2013).

### 2.7 Membrane performance characterization

Membrane rejection properties were tested at 0.1 MPa using 1.0 g/L BSA and 5 g/L PEG-100,000 aqueous solutions, respectively. The concentrations in the feed and the permeate solutions were measured using an Ultraviolet-visible (UV-Vis) spectrophotometer (TU-1901, Purkinje General Instrument Co. Ltd., China), at a wavelength of 280 and 510 nm, respectively. The rejection ( $R$ ) was calculated by the following equation

$$R = 1 - \frac{C_p}{C_f} \quad (3)$$

Where  $C_p$  and  $C_f$  are BSA or PEG concentrations in the permeate and feed solutions, respectively.

### 2.8 The pure water permeation and fouling test experiments

The pure water permeation and fouling experiments were conducted using a lab-scale filtration cell with an effective membrane area of 33.2 cm<sup>2</sup> at ambient temperature. A cross-flow filtration test was operated to evaluate membrane antifouling properties (Meng *et al.* 2012, Kabay *et al.* 2008). Water flux data were collected after the pre-compaction at 0.15 MPa until a steady flux data was obtained. The test interval was 3 min at 0.1 MPa during the whole filtration process. For the first 30 min, pure water flux ( $J_0$ ) was measured at 0.1 MPa, and at least 10 readings were collected in the first step. Then, the feed was replaced by 1 gL<sup>-1</sup> BSA phosphate buffer solution (PBS, 0.01 molL<sup>-1</sup>, pH = 7.4) and water flux ( $J_B$ ) was recorded for another 30 min to examine dynamic fouling resistance. Then, membranes were flushed by pure water for 30 min before another measurement of pure water flux. For the last step, pure water flux ( $J_{re}$ ) was measured similarly to the first step to determine flux recovery ratio ( $R_{FR}$ ). Water flux was obtained as

$$J = \frac{V}{At} \quad (4)$$

Where  $V$  was water permeation volume (L),  $A$  effective membrane area (m<sup>2</sup>),  $t$  filtration time (h).

Flux recovery ratio was defined as

$$R_{FR} = \frac{J_{re}}{J_0} \times 100\% \quad (5)$$

Where  $J_{re}$  was pure water flux after back-flushing (L m<sup>-2</sup> h<sup>-1</sup>),  $J_0$  pure water flux (L m<sup>-2</sup> h<sup>-1</sup>).

### 2.9 Mechanical properties

Blend membranes were cut into 60 × 10 mm as samples of tensile testing, which was performed on a Hounsfield tensile tester (LLY-06, Laizhou Electron Instrument Co., Ltd. China) equipped with a pair of manual wedge-action grips at room temperature. A strain rate of 10 mm·min<sup>-1</sup> was used. Five specimens of each sample were tested and the average value was obtained.

### 2.10 Anti-compression properties

The anti-compression behavior of blend membranes was also performed on the lab-scale filtration cell at ambient temperature. A stable flux was measured and recorded at a raising pressure, membrane thickness was examined by a micrometer caliper.

## 3. Results and discussion

### 3.1 Viscosity of membrane casting solution

Molecular interaction of PVDF and PPTA molecules in membrane casting solutions could be investigated by viscosity measurements as shown in Figs. 1(a) and (b). It can be seen that both casting solutions synthesized by *in situ* polycondensation and solution blending methods exhibited the typical shear thinning behavior of pseudo-plastic fluid and the viscosities greatly increased with the increasing of PPTA concentration (Kiya-Oglu *et al.* 1997). Higher viscosity emerged in casting solution synthesized by *in situ* polycondensation method. This result implied that there was a stronger intermolecular interaction between PVDF and PPTA molecules in *in situ* casting solution which enhanced the entanglement degree of polymer chains resulting in the higher viscosities (Petkova *et al.* 2012). Additionally, different viscosity curves in Fig. 1(a) showed a trivial shear thinning behavior compared with that in Fig. 1(b). This further confirmed that strong molecular interconnection existed in polymer solution prepared by *in situ* polycondensation. The interaction restricted chain movement and sliding with the accelerating of shear rates (Sukitpaneenit and Chung 2009).

### 3.2 Membrane surface compositions

The FT-IR spectra of different blend membranes were shown in Fig. 2. It could be seen that the typical characteristic peak at  $1545.4\text{ cm}^{-1}$  which was assigned to C-N stretching adsorption band of

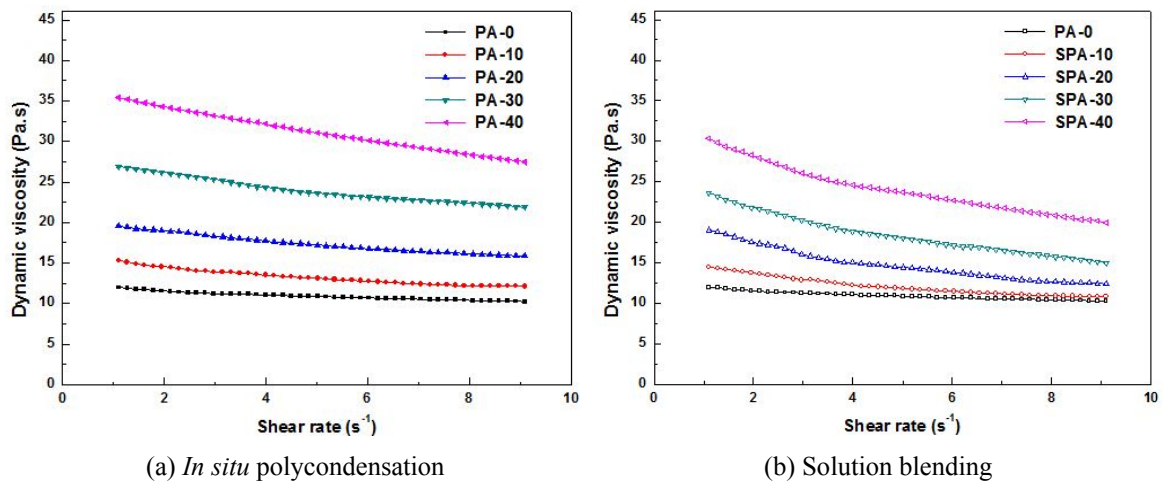


Fig. 1 Dynamic viscosities as a function of shear rates for different casting solution

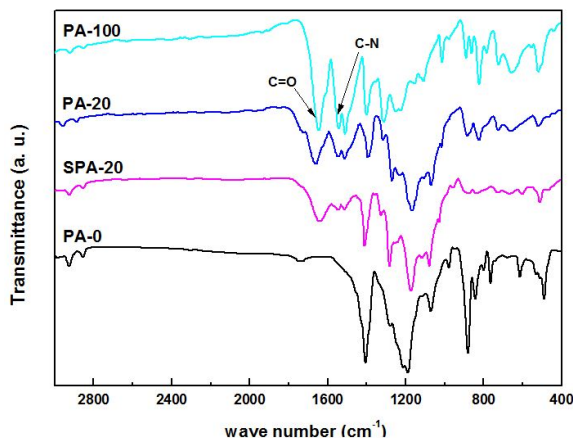
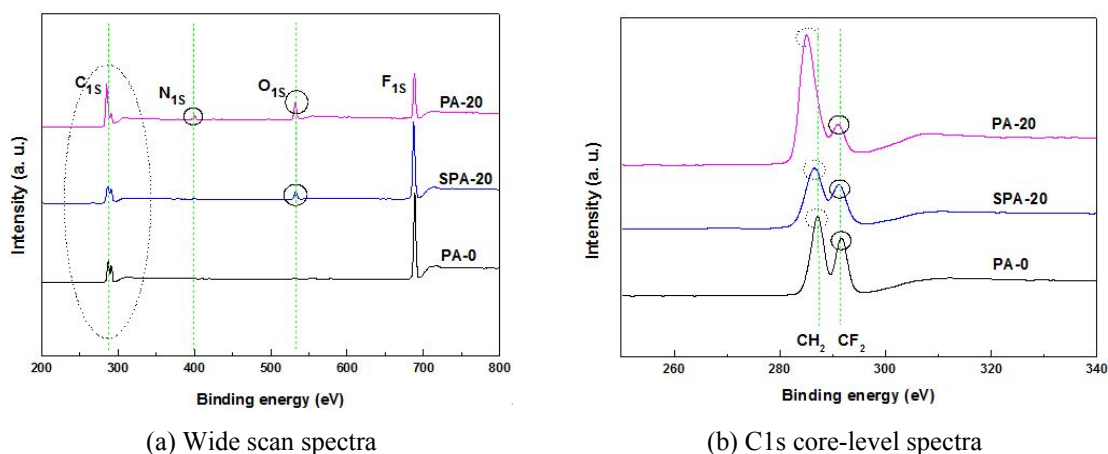


Fig. 2 FT-IR spectra of different blend membranes



(a) Wide scan spectra

(b) C1s core-level spectra

Fig. 3 XPS curves of different membranes

PPTA emerged in the curves of PA-20 and SPA-20 membranes, suggesting that PPTA was successfully synthesized in PVDF matrix (Adamczyk *et al.* 2008). The characteristic peak intensity of *C-N* and *C=O* groups of PA-20 membrane was stronger than that of SPA-20 membrane. This confirmed that more PPTA molecules emerged on the membrane surface which could result in the difference of membrane surface hydrophilicity.

Surface composition of different membranes was further analyzed by XPS. Fig. 3(a) showed the XPS wide scans of different membrane surface. Compare with pure PVDF membrane, two new emission peaks emerged in the curves of blend membranes at approximately 532 and 400 eV which were assigned to O1s and N1s, respectively. This verified the enrichment of the corresponding groups such as *N-H* or *C-N* and *C=O* on membrane surface. The composition of membranes was listed in Table 1. Loh (Loh and Wang 2013) and Feng (Feng *et al.* 2012) point that the hydrophilic groups can migrate to the membrane surface during the phase inversion process to improve membrane hydrophilicity. The PPTA and PVDF molecules in situ blend casting

Table 1 Surface elemental composition of different membranes

Code	Element (at%)			
	O	F <sub>s</sub>	N	C
PA-0	0.56	40.75	0	55.09
PA-20	9.75	18.71	3.53	64.97
SPA-20	6.05	36.48	1.46	52.17

solution were dispersed uniformly dispersed. When the casting solution contacted with the coagulation bath, contact, PPTA can quickly move to the interface, thus leading to the enrichment of hydrophilic groups such as the carbonyl groups on the membrane surface, while more hydrophobic groups such as C-F groups were buried in the membrane matrix, this resulted in the large difference of the F content between PA-20 and SPA-20 membranes.

Oxygen and nitrogen contents increased sharply for PA-20 which could form hydrogen bonds with water molecules and hence resulted in higher hydrophilicity than SPA-20 (Chiang *et al.* 2004). Fig. 3(b) showed the C<sub>1s</sub> core-level spectra of different membrane surface. Two peaks appeared at 287.11 and 292.81 eV in PA-0 curve which represented CH<sub>2</sub> and CF<sub>2</sub> segments of PVDF, respectively (Lin *et al.* 2003). With the incorporation of PPTA, the binding energy of these two peaks in blend membranes both declined. The lowest values were 285.12 and 291.08 eV in PA-20 spectrum with maximal shifts of 1.99 and 1.73eV, respectively. It should be noted that the binding energy decline was much lower in PA-20 than that in SPA-20. These results might be due to the interaction between PPTA molecules and fluorine of PVDF. The fluorine in PVDF acted as an electron donating to hydrogen linked to nitrogen of PPTA molecules and this interaction was much stronger in PA-20 than that in SPA-20 (Lin *et al.* 2003, Kim *et al.* 2003).

### 3.3 Membrane morphology and formation mechanism

The effect of PPTA incorporation on membrane morphologies could be observed by FESEM images in Fig. 4. Surface image of PVDF membrane showed a dense packed surface with few nano-pores. With the addition of PPTA, many micro-pores emerged on membrane surface (PA-20, SPA-20) and gradually enlarged (PA-40, SPA-40). It should be noted that a worm-like aggregation of PPTA crystallization with 2-3  $\mu\text{m}$  length appeared on SPA-40 surface, which might be due to the micro-phase separation as a result of poor polymer compatibility. This phenomenon was confirmed by the shrinkage ratio of SPA-40 as listed in Table 3. More PPTA crystals emerged in PVDF matrix which resulted in a higher shrinkage ratio of membrane. Cross section photo of PVDF membrane showed that lots of cellular pores and short finger-like pores emerged in the top layer and sublayer, respectively. In addition, sponge-like pores uniformly dispersed in the bottom layer of PVDF membrane. With the addition of PPTA (20%), long cellular structure densely covered the top layer and lots of sponge-like pores in the bottom layer disappeared. When PPTA content further increased to 40%, the finger-like pores extended downward to membrane bottom, and macrovoids emerged in the sublayer (PA-40, SPA-40). During the membrane formation process, accelerated demixing generally contributed to a porous skin and even macrovoid sublayer. On the contrary, delayed demixing would initiate a dense and thick top skin. Two aspects of thermodynamic compatibility between polymers and dynamic viscosity of membrane casting solution together determined the demixing rate (Zhao *et al.* 2011). Good compatibility between



polymer components and high casting solution viscosity would result in a delayed demixing rate and vice versa. From the analyses above, membranes prepared by *in situ* polycondensation technique had better polymer compatibility and the corresponding casting solution exhibited a higher viscosity. The situations of solution blend membranes were just the opposite. When a small amount of PPTA was added (20%), both viscosities of casting solutions synthesized by these two methods were low. Therefore, thermodynamic compatibility played a major role in the solution demixing process. Compared with PA-20, poor compatibility between polymers resulted in an accelerated demixing rate and a more porous structure in SPA-20. However, when PPTA concentration increased over 20wt%, the combination of poor thermodynamic compatibility and lower dynamic viscosity promoted the emergence of instantaneous demixing with a larger macrovoid structure formed in SPA-40.

The values of average pore size and porosity of different membranes were shown in Tables 2-3. It could be seen that all blend membranes had larger pore size and higher porosity than PVDF membrane. With the increasing of PPTA content, both pore size and porosity increased sharply and then leveled off. This was because that the incorporation of PPTA significantly accelerated phase separation process at low PPTA content (20wt%). However, when PPTA content increased over 20wt%, the higher viscosity of polymer dopes delayed the exchange rate of solvent-nonsolvent and the accelerated demixing rate gradually slowed down. Thus, the increasing of pore size and porosity leveled off. In addition, the solution blend membranes showed bigger pore size and higher porosity than *in situ* blend membranes. This was attributed to the faster micro-phase separation during the demixing process of the solution blend membrane formation. When PPTA content was higher, the rigid PPTA molecules acted as the rigid supports in the membrane matrix. This resulted in the decrease of membrane shrinkage ratio. Compared with the *in situ* blend membrane, the shrinkage ratio of solution blend membrane is bigger. This was mainly because the PPTA molecules can be uniformly dispersed in the *in situ* membrane matrix while more crystallization emerged in solution blend membrane matrix polymer due to the poor compatibility

Table 2 Performance parameters of PVDF/PPTA *in situ* blend membranes

Samples	Porosity (%)	Average pore size (nm)	Thickness ( $\mu\text{m}$ )	Shrinkage ratio (%)	Contact angle ( $^{\circ}$ )
PA-0	55.6 $\pm$ 2.3	96 $\pm$ 3	260 $\pm$ 6	22 $\pm$ 2	88 $\pm$ 1.2
PA-10	64.8 $\pm$ 1.4	205 $\pm$ 9	285 $\pm$ 8	13 $\pm$ 4	74 $\pm$ 1.8
PA-20	69.1 $\pm$ 1.6	281 $\pm$ 10	322 $\pm$ 6	10 $\pm$ 2	62 $\pm$ 2.1
PA-30	70.7 $\pm$ 0.9	308 $\pm$ 7	358 $\pm$ 2	13 $\pm$ 2	65 $\pm$ 2.2
PA-40	72.1 $\pm$ 2.1	294 $\pm$ 4	375 $\pm$ 5	15 $\pm$ 1	69 $\pm$ 1.8

Table 3 Performance parameters of PVDF/PPTA solution blend membranes

Samples	Porosity (%)	Average pore size (nm)	Thickness ( $\mu\text{m}$ )	Shrinkage ratio (%)	Contact angle ( $^{\circ}$ )
PA-0	55.6 $\pm$ 2.3	96 $\pm$ 3	260 $\pm$ 6	22 $\pm$ 2	88 $\pm$ 1.2
SPA-10	70.1 $\pm$ 0.8	231 $\pm$ 6	298 $\pm$ 8	16 $\pm$ 2	77 $\pm$ 3.3
SPA-20	74.8 $\pm$ 1.2	309 $\pm$ 7	340 $\pm$ 11	13 $\pm$ 4	70 $\pm$ 2.1
SPA-30	76.7 $\pm$ 1.9	334 $\pm$ 9	373 $\pm$ 6	15 $\pm$ 3	73 $\pm$ 1.6
SPA-40	78.9 $\pm$ 1.7	368 $\pm$ 4	325 $\pm$ 4	17 $\pm$ 1	75 $\pm$ 2.3

between polymer pairs. Consequently, the membrane shrinkage ratio of solution blend membrane became larger.

### 3.4 Membrane hydrophilicity and hydration capability

Membrane surface hydrophilicity was evaluated using water contact angle (WCA) measurements. The WCA values of different membranes were shown in Tables 2-3. It could be obviously seen that WCA values of all blend membranes were lower than that of PVDF membrane, which implied that the addition of hydrophilic PPTA improved wetting ability of blend membrane surface. Compared to *in situ* blend membranes, solution blend membranes showed a larger WCA value. Membrane surface roughness and intrinsic hydrophilicity of the material itself are the two major factors affecting the WCA value (Yang *et al.* 2010). Membrane surface roughness can be reflected by the surface pore size to some extent that a larger pore size implies a higher surface roughness (Liu *et al.* 2012b, Gao *et al.* 2013). It could be seen from Tables 2-3 that the difference of pore size between *in situ* blend membrane and solution blend membrane was smaller. All blend membranes belonged to ultrafiltration membrane. Thus, the intrinsic hydrophilicity of the material itself became the major factor affecting membrane surface hydrophilicity. More hydrophilic PPTA molecules enriched on *in situ* blend membrane surface which resulted a smaller WCA value than that of solution blend membrane. Souza pointed (Souza and Baird 1996) that a lower WCA value implied a better compatibility between the polymer pairs which was determined by the higher work of adhesion. The optimization of hydrophilicity was achieved when PPTA content was 20wt%. This suggested the polymer pairs at this proportion in blend membranes had the best compatibility.

Fig. 5 showed the hydration capacity of different membranes. It can be seen that the hydration capacity was gradually increased from 550 to 760 mg/cm<sup>3</sup> when 40wt% PPTA was added. This indicated with the increasing of PPTA content the whole wettability of membranes was improved. The entrapment of water inside the polymer matrix became favorable. This was attributed to the presence of amide groups in the bulk which formed hydrogen bonds with water molecules.

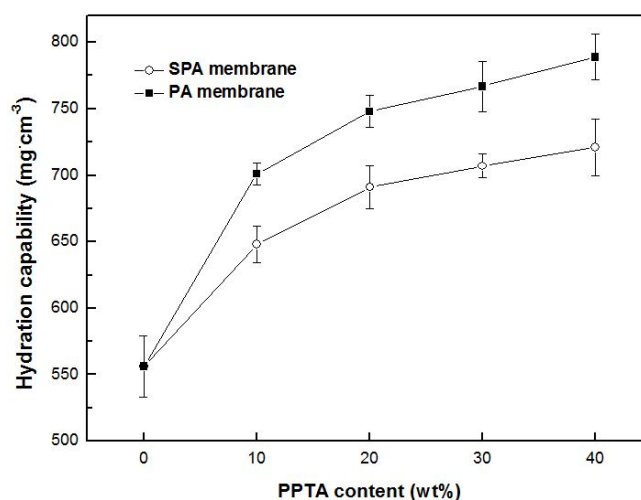


Fig. 5 The hydration capability of different membranes

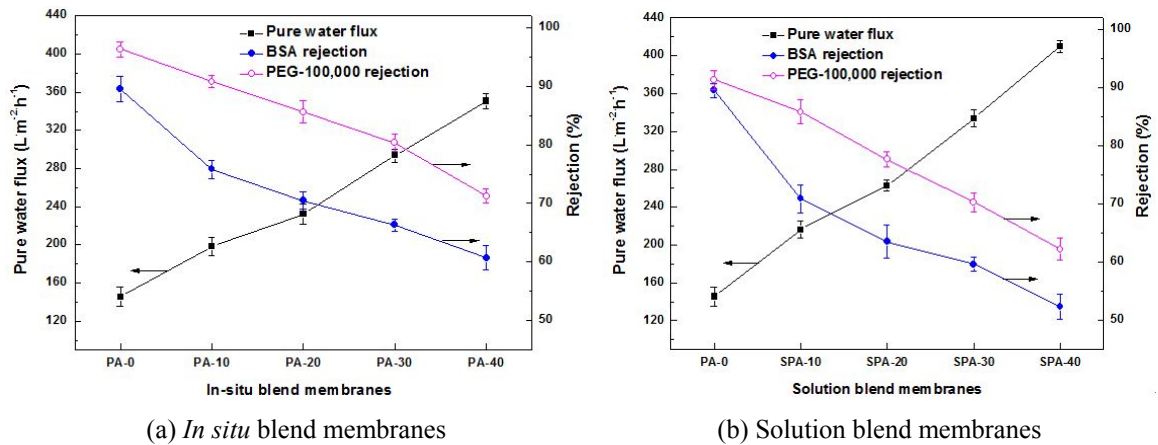


Fig. 6 BSA and PEG100,000 rejections of different membranes

### 3.5 Characterization of membrane performance

#### 3.5.1 Membrane pure water flux and rejection

Fig. 6 showed the variations of pure water flux and the rejections of BSA and PEG-100, 000 of different blend membranes. It could be seen that the permeability and rejection of blend membranes were greatly influenced by the introduction of PPTA. With the increasing of PPTA content, the permeate flux gradually increased and the rejections of BSA and PEG-100, 000 showed the opposite trends. It was due to the increasing of surface pore size as listed in Tables 2-3. In view of its proper rejection and high flux, PVDF/PPTA blend membranes prepared in this study were thought to be appropriate for the application in waster-water treatment and bio-separation.

#### 3.5.2 Membrane antifouling properties

The improvement of membrane antifouling properties is beneficial to increase separation efficiency, reduce operating cost and prolong the duration time (Yeh *et al.* 2012). BSA fouling as non-specific adsorption was usually used to evaluate membrane antifouling properties. Fig. 7 showed water flux changes with filtration time of different membranes. It could be seen from Fig. 7 that blend membranes had a water permeability dramatically higher than that of PVDF membrane. During the filtration cycles, all the membranes showed an inevitable flux decline which was attributed to the continuous protein block on surface pores and cake layer formation on membrane surface. *In situ* blend membranes showed a lower flux than that of solution blend membranes at the same proportion. Flux recovery of pure water after washing was investigated to evaluate antifouling properties of different blend membranes as shown in Fig. 8. It could be seen that both *in situ* blend membranes and solution blend membranes had higher  $R_{FR}$  values than that of PVDF membrane, suggesting that the incorporation of PPTA in blend membranes enhanced membrane antifouling properties. With the increasing of PPTA content,  $R_{FR}$  values increased firstly and then decreased. The similar results were obtained in other blending systems (polysulfone/polyvinyl pyrrolidone/polyaniline, PSF/PVP/PANI) (Zhao *et al.* 2011).

Membrane surface hydrophilicity and surface pore size were two main factors affecting membrane antifouling properties. Generally, membrane surface with higher hydrophilicity and

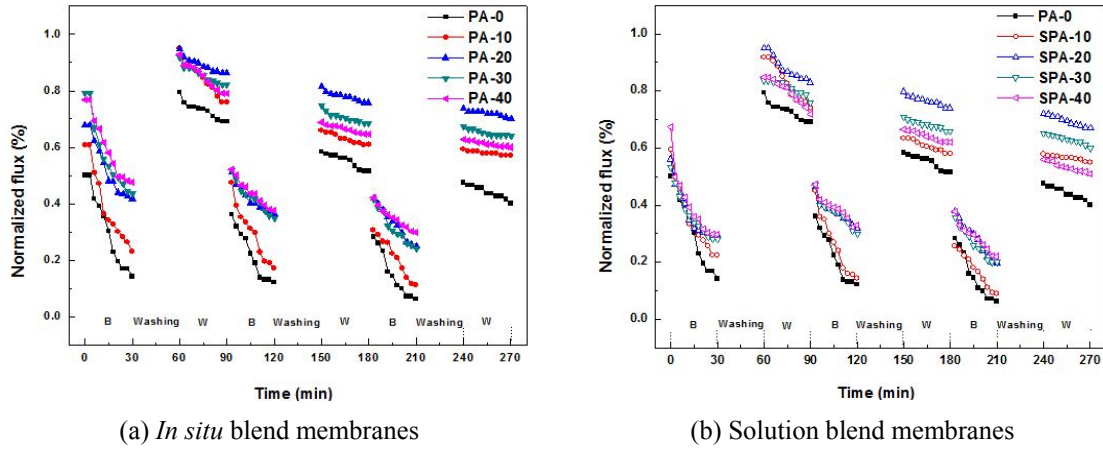


Fig. 7 Water flux as a function of filtration time of different membranes (*W*: pure water flux, *B*: the BAS/PBS solution flux)

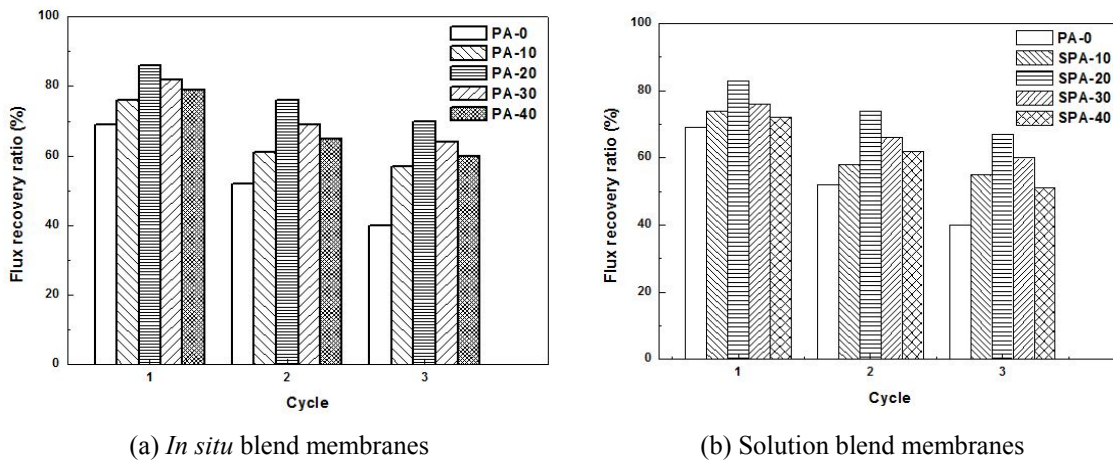


Fig. 8 Flux recovery ratio ( $R_{FR}$ ) values of different blend membranes (1, 2, 3 represent the times of cycles)

smaller pore size possessed better antifouling properties (Li and Chen 2004). It could be found that the general change trends of antifouling property of different blend membranes were similar to that of surface hydrophilicity, which indicated that the hydrophilicity of PVDF/PPTA blend membranes determined their antifouling properties. It could also be observed that the difference of flux recovery ratio between *in situ* blend membranes and solution blend membranes increased when PPTA content increased over 20wt%. This could be explained with the results in Tables 2-3 that the pore size of solution blend membranes was much larger than the counterparts of *in situ* blend membranes at high PPTA concentration, which exacerbated protein adsorption and blocking on solution blend membrane surface.

### 3.5.3 Membrane mechanical properties

Membrane mechanical properties were examined by the measurements of their tensile strength

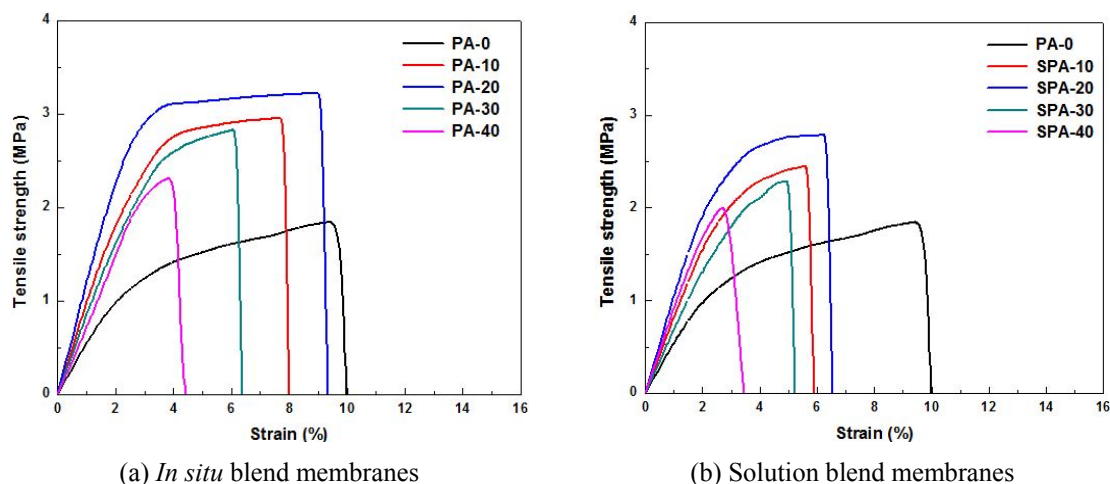


Fig. 9 Stress-strain curves of different membranes

and elongation-at-break. Figs. 9(a) and (b) showed the stress-strain curves of *in situ* blend membranes and solution blend membranes, respectively. Generally, a massive introduction of external components in porous ultrafiltration membranes will cause the decline of mechanical strength (Yuliwati *et al.* 2011). However, Fig. 9 showed that all blend membranes exhibited enhanced tensile strength than PVDF membrane and with the increase of PPTA concentration, tensile strength increased firstly and then decreased. When PPTA content was 20wt%, blend membranes prepared by different blending methods showed the respective highest tensile strength. Additionally, *in situ* blend membranes displayed higher tensile strength than solution blend membranes at the same PPTA concentration. This was because during the *in situ* blending process, the incorporation of PPTA molecules in PVDF matrix could prevent stacking and aggregation of PVDF and these two polymer components entangled with each other due to the strong molecular interaction. Consequently, the interfacial adhesion between different components in *in situ* blend membranes was stronger. PA-20 exhibited the best mechanical properties despite the small decline of elongation-at-break which was acceptable in practical application. The results again demonstrated that good compatible blend membranes could be obtained by *in situ* polycondensation technique and the compatibility played a vital role in determining the mechanical strength of ultrafiltration membranes.

### 3.5.4 Membrane anti-compression properties

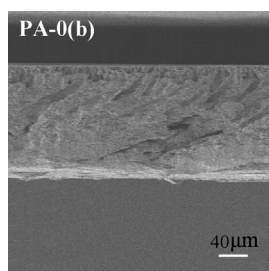
The changes of pore volumes after being pressurized at 0.4 MPa were measured by Flow Porometer and the results were listed in Table 4. It could be seen that for pristine PVDF membrane, an initial pore volume of about  $0.75\text{cm}^3\text{g}^{-1}$  was determined. After being pressurized 2 h at 0.4 MPa, the volume decreased to  $0.32\text{cm}^3\text{g}^{-1}$  which was about 43% of the initial pore volume. With the incorporation of PPTA, the pore volumes were also decreased with a reduction of 12 and 20% of pristine PA-20 and SPA-20 membranes, respectively. The decline was much smaller than that of PVDF membrane. This indicated that the pore structure of PVDF/PPTA blend membranes was not changed seriously which could be obviously seen in FESEM pictures. Fig. 10 showed the cross-sectional pictures of PVDF and different blend membranes. It could be observed that after

the pressure treatment, the asymmetric finger-like pores of PVDF membrane as shown in Fig. 10(PA-0) were strongly squeezed and the membrane thickness was reduced nearly 20%. The top layer of SPA-20 was tightly compressed and the finger-like pores were greatly deformed. For PA-20, the caverns and macrovoids were also squeezed while the top of finger-like pores seemed to be simply densified and the original shape was well maintained. The reduction of blend membrane thickness was about 10% which suggested that PPTA molecules with rigid chains greatly improved the anti-compression behavior. The deformation of PVDF/PPTA blend membranes was mainly attributed to the pore size and the dispersal of rigid PPTA molecules. PPTA molecules were uniformly dispersed in *in situ* blend membranes and the pore size was smaller than solution blend membranes. These resulted in the reduction of the domains of stress concentration under a certain pressure.

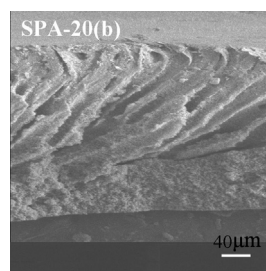
Membrane deformation could be well reflected by the variations of membrane thickness after pressuring. It could be seen from Fig. 11 that membrane thickness was significantly changed with the raising of feeding pressure. When the feeding pressure increased to 0.2 MPa, the thickness of PVDF membrane was greatly reduced, then remained stable. With the raising of the pressure

Table 4 Pore volumes of pristine and pressurized membranes (at 0.4 MPa for 2 h)

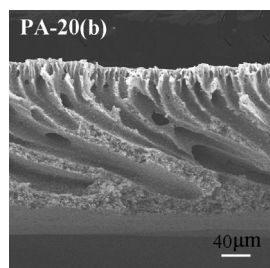
Membrane	Pore volume of pristine membrane ( $\text{cm}^3 \cdot \text{g}^{-1}$ )	Pore volume of pressurized membrane ( $\text{cm}^3 \cdot \text{g}^{-1}$ )	Decrease of pore volume (%)
PA-0	0.75	0.32	57
PA-20	1.68	1.45	12
SPA-20	1.86	1.49	20



(a) PVDF membrane



(b) Solution blend membrane



(c) *In situ* blend membrane

Fig. 10 FESEM images of different membranes after pressure treatment at 0.4 MPa for 2 h ( $\times 250$ )

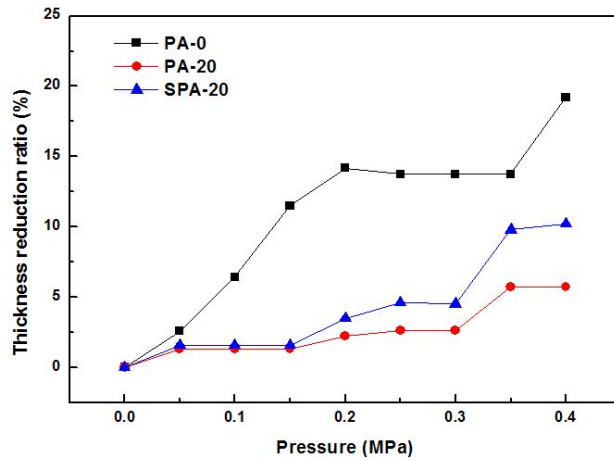


Fig. 11 Variations of membrane thickness at different pressure

to about 0.4 MPa, the thickness continued to reduce greatly which was about 20%. The changes of blend membrane thickness showed different trends. When the pressure rose to 0.35 MPa, the film thickness is decreased only about 5-10%.

The effects of pore deformation on pure water flux and PEG-100, 000 rejections of different membranes were illustrated in Fig. 12 and Table 5. It could be seen in Fig. 12 that the pure water flux increased significantly with the raising of feeding pressure to 0.2 MPa. From the data in Table 5, 58.3% reduction of PEG rejection occurred after pressuring at 0.4 MPa which indicated that membrane surface pores were greatly deformed especially at 0.2 MPa. The pure water flux of blend membranes increased steadily with the raising of feeding pressure. And the PEG rejection also had a small increase. These results suggested that the blend membrane pore was not damaged, but densely compacted. Obviously, the *in situ* blend membrane exhibited a higher anti-compression property.

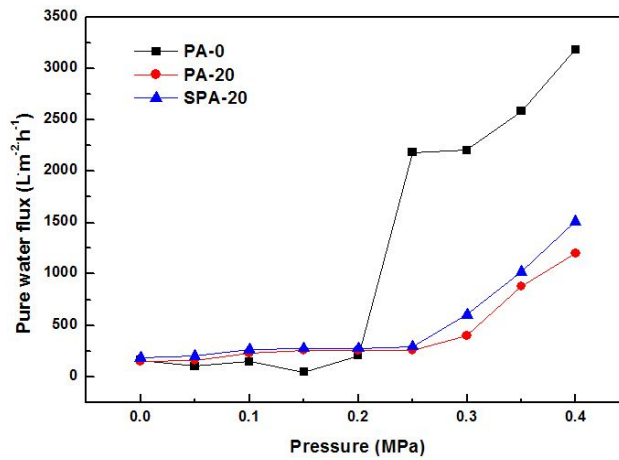


Fig. 12 Variations of pure water flux of different membranes at different pressure

Table 5 PEG 100,000 rejection of pristine and pressurized membranes (at 0.4 MPa for 2 h)

Membrane	PEG rejection of pristine membrane ( $\text{cm}^3\cdot\text{g}^{-1}$ )	PEG rejection of pressurized membrane ( $\text{cm}^3\cdot\text{g}^{-1}$ )	Decrease of PEG rejection (%)
PA-0	96.3	40.2	+58.3
PA-20	85.6	94.4	-10.2
SPA-20	77.6	91.7	-18.2

#### 4. Conclusions

Hydrophilic PVDF/PPTA blend membranes were prepared via a novel blending method of *in situ* polycondensation. The reduction of  $C_{1s}$  binding energy in XPS curves verified that stronger intermolecular interactions especially hydrogen bonds between PVDF and PPTA molecules existed in *in situ* blend membranes. The higher viscosity and trivial strain thinning behavior of casting solution synthesized by *in situ* polycondensation further confirmed that excellent polymer compatibility was obtained by *in situ* polycondensation method. *In situ* blend membranes exhibited higher hydrophilicity and stronger mechanical properties which were attributed to the enrichment of PPTA on membrane surface and their better polymer compatibility, respectively. Higher casting solution viscosities and better polymer compatibility in *in situ* blend membranes induced a delayed demixing and hence formed a membrane structure with smaller pore size. The smaller pore size and improved hydrophilicity together caused an improved antifouling property of *in situ* blend membranes. Additionally, the anti-compression property of *in situ* blend membranes was greatly improved. Considering all the analyses above, the resulted PVDF/PPTA *in situ* blend membranes were promising for the application in wastewater treatments or bio-separation.

#### References

- Adamczyk, N.M., Dameron, A.A., George, S.M. (2008), "Molecular Layer Deposition of Poly(*p*-phenylene terephthalamide) Films Using Terephthaloyl Chloride and *p*-Phenylenediamine", *Langmuir*, **24**(5), 2081-2089.
- Chiang, C.Y., Reddy, M.J. and Chu, P.P. (2004), "Nano-tube  $\text{TiO}_2$  composite PVdF/LiPF<sub>6</sub> solid membranes", *Solid State Ionics*, **175**(1-4), 631-635.
- Feng, S.G., Shang, Y.M., Wang, S.B., Xie, X.F., Wang, Y.Z., Wang, Y.W and Xu, J.M. (2010), "Novel method for the preparation of ionically crosslinked sulfonated poly (arylene ether sulfone)/ polybenzimidazole composite membranes via *in situ* polymerization", *J. Membr. Sci.*, **346**(1), 105-112.
- Feng, X., Guo, Y.F., Chen, X., Zhao, Y.P., Li, J.X., He, X.L. and Chen, L. (2012), "Membrane formation process and mechanism of PVDF-g-PNIPAAm thermo-sensitive membrane", *Desalination*, **290**, 89-98.
- Fu, T.Z., Zhao, C.J., Zhong, S.L., Zhang, G., Shao, K., Zhang, H.Q., Wang, J. and Na, H. (2007), "SPEEK/epoxy resin composite membranes *in situ* polymerization for direct methanol fuel cell usages", *J. Power Sources*, **165**(2), 708-716.
- Gao, X.L., Wang, H.Z., Wang, J., Huang, X. and Gao, C.J. (2013), "Surface-modified PSf UF membrane by UV-assisted graft polymerization of capsaicin derivative moiety for fouling and bacterial resistance", *J. Membr. Sci.*, **445**, 146-155.
- Han, M.M., Zhang, G., Li, M.Y., Wang, S., Liu, Z.G., Li, H.T., Zhang, Y., Xu, D., Wang, J., Ni, J. and Na, H. (2011), "Sulfonated poly(ether ether ketone)/ polybenzimidazole oligomer/epoxy resin composite membranes *in situ* polymerization for direct methanol fuel cell usages", *J. Power Sources*, **196**(23), 9916-

9923.

- Hashim, N.A., Liu, F., Moghareh, M.R. and Li, K. (2012), "Chemistry in spinning solutions: Surface modification of PVDF membranes during phase inversion", *J. Membr. Sci.*, **415**, 399-411.
- Hegde, C., Isloor, A.M., Padaki, M., Ismail, A.F. and Lau, W.J. (2012), "New CPS-PPEES blend membranes for CaCl<sub>2</sub> and NaCl rejection", *Membr. Water Treat., Int. J.*, **3**(1), 25-34.
- Huang, Y.J., Ye, Y.S., Syu, Y.J., Hwang, B.J. and Chang, F.C. (2012), "Synthesis and characterization of sulfonated polytriazole-clay proton exchange membrane by *in situ* polymerization and click reaction for direct methanol fuel cells", *J. Power Sources*, **208**, 144-152.
- Ji, Y.L., Ma, J.H. and Liang, B.R. (2005), "*In situ* polymerization and *in situ* compatibilization of polymer blends of poly(2,6-dimethyl-1,4-phenylene oxide) and polyamide 6", *Mater. Lett.*, **59**(16), 1997-2000.
- Kabay, N., Bryjak, M., Schlosser, S., Kitis, M., Avlonitis, S., Matejka, Z., Al-Mutaz, I. and Yuksel, M. (2008), "Adsorption-membrane filtration (AMF) hybrid process for boron removal from seawater: An overview", *Desalination*, **22**(1-3), 338-48.
- Kim, K.J., Cho, H.W. and Yoon, K.J. (2003), "Effect of P(MMA-co-MAA) compatibilizer on the miscibility of nylon 6/PVDF blends", *Eur. Polym. J.*, **39**(6), 1249-1265.
- Kiya-Oglu, V.N., Rozhdestvenskaya, T.A. and Serova, L.D. (1997), "Rheological properties of liquid-crystalline solutions of poly(p-phenylene terephthalamide) and behavior of the jet in spinning through an air space", *Fiber Chem.*, **29**(2), 81-86.
- Knijnenberg, A., Bos, J. and Dingemans, T.J. (2010), "The synthesis and characterisation of reactive poly(p-phenylene terephthalamide)s: A route towards compression stable aramid fibers", *Polym.*, **51**(9), 1887-1897.
- Li, C.W. and Chen, Y.S. (2004), "Fouling of UF membrane by humic substance: effects of molecular weight and powder-activated carbon (PAC) pre-treatment", *Desalination*, **170**(1), 59-67.
- Lin, D.J., Chang, C.L., Huang, F.M. and Cheng, L.P. (2003), "Effect of salt additive on the formation of microporous poly(vinylidene fluoride) membranes by phase inversion from LiClO<sub>4</sub>/Water/DMF/PVDF system", *Polym.*, **44**(2), 413-422.
- Liu, F., Hashim, N.A., Liu, Y.T. and Abed, M.R. (2011), "Progress in the production and modification of PVDF membranes", *J. Membr. Sci.*, **375**(1-2), 1-27.
- Liu, F., Tao, M.M. and Xue, X.L. (2012a), "A novel method of combining *in situ* polymerization and non-solvent assisted thermally induced micro-phase separation to improve membrane hydrophilicity", *Procedia Eng.*, **44**, 1433-1434.
- Liu, B.C., Chen, C., Zhang, W., Crittenden, J. and Chen, Y.S. (2012b), "Low-cost antifouling PVC ultrafiltration membrane fabrication with Pluronic F 127: Effect of additives on properties and performance", *Desalination*, **307**, 26-33.
- Loh, C.H. and Wang, R. (2013), "Insight into the role of amphiphilic pluronic block copolymer as pore-forming additive in PVDF membrane formation", *J. Membr. Sci.*, **446**, 492-503.
- Madaeni, S.S., Zinadini, S. and Vatanpour, V. (2011), "A new approach to improve antifouling property of PVDF membrane using *in situ* polymerization of PAA functionalized TiO<sub>2</sub> nanoparticles", *J. Membr. Sci.*, **380**(1-2), 155-162.
- Meng, J.Q., Yuan, T., Kurth, C.J., Shi, Q. and Zhang, Y.F. (2012), "Synthesis of antifouling nanoporous membranes having tunable nanopores via clickchemistry", *J. Membr. Sci.*, **401-402**, 109-117.
- Nasef, M.M. and Hegazy, E.S. (2004), "Preparation and applications of ion exchange membranes by radiation-induced graft copolymerization of polar monomers onto non-polar films", *Prog. Polym. Sci.*, **29**(6), 499-561.
- Pang, R.Z., Li, J.S., Wei, K.J. and Shen, J.Y. (2011), "*In situ* preparation of Al-containing PVDF ultrafiltration membrane via sol-gel process", *J. Colloid Interf. Sci.*, **364**(2), 373-378.
- Petkova, R., Tcholakova, S. and Denkov, N.D. (2012), "Foaming and foam stability for mixed polymer-surfactant solutions: effects of surfactant type and polymer charge", *Langmuir*, **28**(11), 4996-5009.
- Rao, Y., Waddon, A.J. and Farris, R.J. (2001), "The evolution of structure and properties in poly(p-phenylene terephthalamide) fibers", *Polym.*, **42**(13), 5925-5935.

- Shi, H.Y., Liu, F. and Xue, L.X. (2013), "Fabrication and characterization of antibacterial PVDF hollow fibre membrane by doping Ag-loaded zeolites", *J. Membr. Sci.*, **437**, 205-215.
- Souza, P. and Baird, D.G. (1996), "In situ composites based on blends of a poly(ether imide) and thermotropic liquid crystalline polymers under injection moulding conditions", *Polymer*, **37**(10), 1985-1997.
- Sukitpaneent, P. and Chung, T.S. (2009), "Molecular elucidation of morphology and mechanical properties of PVDF hollow fiber membranes from aspects of phase inversion, crystallization and rheology", *J. Membr. Sci.*, **340**(1-2), 192-205.
- Vaughan, B., Peter, J., Marand, E., Bleha, M. and Bleha, M. (2008), "Transport properties of aluminophosphate nanocomposite membranes prepared by *in situ* polymerization", *J. Membr. Sci.*, **316**(1-2), 153-163.
- Woo, J.B., Won, H.J. and Yun, H.P. (2003), "Preparation of polystyrene/polyaniline blends by *in situ* polymerization technique and their morphology and electrical property", *Synth. Met.*, **132**(3), 239-244.
- Yang, Y.F., Li, Y., Li, Q.L., Wan, L.S. and Xu, Z.K. (2010), "Surface hydrophilization of microporous polypropylene membrane by grafting zwitterionic polymer for anti-biofouling", *J. Membr. Sci.*, **362**(1-2), 255-264.
- Yeh, H.M., Ho, C.D. and Li, C.H. (2012), "Effects of ring number and baffled-ring distances on ultrafiltration in the tubular membrane inserted concentrically with a ring rod", *Membr. Water Treat., Int. J.*, **3**(1), 51-62.
- Yuliwati, E., Ismail, A.F., Matsuura, T., Kassim, M.A. and Abdullah, M.S. (2011), "Effect of modified PVDF hollow fiber submerged ultrafiltration membrane for refinery wastewater treatment", *Desalination*, **283**, 214-220.
- Zhang, P.Y., Xu, Z.L., Yang, H., Wei, Y.M. and Wu, W.Z. (2013), "Fabrication and characterization of PVDF membranes via an *in situ* free radical polymerization method", *Chem. Eng. Sci.*, **97**, 296-308.
- Zhao, Y.H., Zhu, B.K., Kong, L. and Xu, Y.Y. (2007), "Improving hydrophilicity and protein resistance of poly(vinylidene fluoride) membranes by blending with amphiphilic hyper branched star polymer", *Langmuir*, **23**(10), 5779-5786.
- Zhao, S., Wang, Z., Wei, X., Tian, X.X., Wang, J.X., Yang, S.B. and Wang, S.C. (2011), "Comparison study of the effect of PVP and PANI nanofibers additives on membrane formation mechanism, structure and performance", *J. Membr. Sci.*, **385-386**, 110-122.